Boundary-Layer Meteorol (2007) 122:149–165
DOI 10.1007/s10546-006-9097-x

ORIGINAL PAPER

Influence of surface heterogeneity on scalar dissimilarity in the roughness sublayer

Christopher A. Williams · Todd M. Scanlon · John D. Albertson

Received: 20 October 2005 / Accepted: 15 May 2006 /
Published online: 11 November 2006

Abstract While it is generally known that surface heterogeneity weakens the application of Monin–Obukhov similarity (MOS), few studies have investigated how seasonal changes in the degree of surface heterogeneity at a particular site may influence the validity of the similarity application. Exploiting seasonal changes in forest function associated with senescence, we conduct a unique evaluation of the effects of surface heterogeneity on the validity of similarity theory at two sites through time. Using high frequency (10 Hz) velocity and scalar time series collected within the roughness sublayer over mixed hardwood deciduous and coniferous forests during both periods of peak leaf area and senescence of deciduous foliage, we examined conformity with proposed universal flux-variance predictions and agreement amongst normalized standard deviations of different scalars (temperature, water vapour and carbon dioxide concentrations). Normalized scalar standard deviations were elevated above MOS flux-variance predictions, with more pronounced deviations observed during and following senescence, particularly in the case of CO_2. Power-law scaling of normalized standard deviations as a function of stability was upheld and robust to seasonal changes in surface heterogeneity. However, dissimilarity of normalized standard deviations for the scalars increased during senescence, as heterogeneity in the source/sink field increased. Scalewise decomposition of scalar time series using wavelet analysis indicated that correlations between scalars were conservative through much of the inertial cascade but decayed for eddies <10 m. Senescence lowered corre-

C. A. Williams (✉)
Natural Resource Ecology Laboratory, Colorado State University, Fort Collins, CO, 80523-1499, USA
e-mail: caw@nrel.colostate.edu

C. A. Williams · J. D. Albertson
Department of Civil and Environmental Engineering, Duke University, Durham, NC, 27708-0287, USA

T. M. Scanlon
Department of Environmental Sciences, University of Virginia, Charlottesville, VA 22904-4123, USA

lations between scalars over a wide range of eddy sizes. These results demonstrate how seasonal changes in surface physiology can cause a temporal production of heterogeneity in the source/sink field, thus weakening similarity applications in the roughness sublayer.

Keywords Flux-variance prediction · Monin–Obukhov similarity theory · Scalar transport · Wavelet analysis

1 Introduction

Monin–Obukhov similarity (MOS) theory remains an important tool for studies of the atmospheric surface layer (ASL), and states that for a turbulent, stationary flow over a horizontally homogeneous surface, the velocity and scalar gradients, variances, and covariances are universal when normalized by the appropriate scaling parameters. Since its introduction by Monin and Obukhov (1954) and Obukhov (1960), it has been used widely to estimate surface fluxes of mass and energy from measurements of flow statistics, with success demonstrated in ASL applications of both the gradient method (Businger et al. 1971; Dyer 1974; Cellier and Brunet 1992; Simpson et al. 1998; Mölder et al. 1999) and the variance method (Tillman 1972; Wesely 1988; Weaver 1990; Lloyd et al. 1991; de Bruin et al. 1993; Padro 1993; Albertson et al. 1995; Katul et al. 1995, 1996; Hsieh et al. 1996). Empirically-based similarity functions were proposed to describe the effect of atmospheric stability on these normalized flow statistics, obtained from measurements conducted in the ASL under ideal conditions, and enabling estimates of surface exchanges based solely on knowledge of atmospheric stability (e.g. Monin and Yaglom 1971).

Similarity theory leads to an expectation of similar transport for passive scalars (Hill 1989), where passive scalars are those transported without dynamically affecting the turbulent flow from effects such as buoyancy (Warhaft 2000). So-called similar scalars have, by definition, equal normalized statistics and equal velocity-scalar correlation coefficients (Hill 1989; Dias and Brutsaert 1996). Similar scalars may also have perfectly correlated fluctuations; however we note that this is not a necessary condition for scalar transport to be similarly scaled, as discussed by both Katul et al. (1995) and McNaughton and Laubach (1998). A subset of MOS applications relies directly on the implicit assumption of scalar similarity, making it possible, for example, to estimate the exchange of scalars for which fast response sensors are not readily available, based on the exchange of more easily measured scalars (Monin and Yaglom 1971; Dias and Brutsaert 1996).

The MOS theory, with its assumption of horizontal homogeneity, applies to the ASL, well above the roughness sublayer (RSL) (Garratt 1978; Brutsaert 1982; Kaimal and Finnigan 1994). However, despite departure from ideal MOS conditions, many micrometeorological techniques that rely on some subset of similarity statistics are often employed in the RSL due to logistical limitations such as tower height, fetch, or instrument resolution. The RSL is characterized by a local flow that is influenced by individual surface roughness elements (Raupach et al. 1996; Mahrt 2000), and empirical evidence suggests that the RSL extends up to 1.5 to 3 times the canopy height, h (Cellier and Brunet 1991; Kaimal and Finnigan 1994; Rotach 1999) and that it possesses an enhanced turbulent diffusivity vis-à-vis MOS. Additional disagreement in some RSL applications between measured statistics and proposed universal functions,

as well as disagreement between normalized statistics for different scalars, has led us to consider how heterogeneity (i.e. patchiness) in surface cover further weakens the applicability of similarity theory to the RSL.

Most studies that have investigated the impact of surface heterogeneity on similarity examine the effect of different levels of heterogeneity by comparing results across a range of different sites, often with ASL observations (e.g., Weaver 1990; Lloyd et al. 1991; De Bruin et al. 1993; Padro 1993; Katul et al. 1995, 1996; Roth and Oke 1995; Andreas et al. 1998). In this study, we evaluate the similarity theory applied in the RSL at two individual sites each with mixed deciduous–coniferous forests as they progress from periods of full leaf area into periods of deciduous leaf senescence and abscission. Seasonal onset of senescence introduces a *temporal production of patchiness* in canopy exchange surfaces as the loss of deciduous foliage reduces canopy density and increases the heterogeneity of the source/sink distributions of temperature (T), carbon dioxide (c), and water vapour (q). We quantify the effects of these changes in forest structure and function on the degree to which MOS applies in the RSL during peak leaf area through the senescence of deciduous foliage. Before identifying the specific questions of this work, we review RSL applications of MOS theory and the role of heterogeneity in weakening these applications.

1.1 Weaknesses in RSL application of MOS theory

The universal MOS functions proposed to account for the effect of stability on transport in the ASL tend to underestimate eddy diffusivities in the RSL, resulting in underestimated surface layer exchanges from measured mean vertical profiles of velocity and scalars (Thom et al. 1975; Garratt 1978, Raupach 1979; Denmead and Bradley 1985; Högstrom et al. 1989; Cellier and Brunet 1992; Mölder et al. 1999). Normalized scalar standard deviations obtained from measurements in the RSL also tend to be elevated above proposed universal forms, in this case flux-variance similarity functions (Katul et al. 1995; Roth and Oke 1995; Rotach 1999). Heterogeneity in the scalar source/sink field can contribute to the elevation of measured normalized standard deviations, as the sampling of air parcels that interact with the heterogeneous source/sink field adds temporal variance that is not necessarily related to mean surface exchange (vertical flux) (Weaver 1988; Katul et al. 1995). Overestimation of sensible and latent heat fluxes associated with the elevated normalized standard deviations has been consistent across many studies conducted in the RSL over heterogeneous surfaces, including grasslands, forests, desert, a wetland, and an urban environment (e.g. Weaver 1990; Padro 1993; Katul et al. 1995). In this study, we will refer to the symptom of departure of measured statistics (at a particular site) from the proposed universal ASL forms as *nonuniversal* behaviour.

In addition to nonuniversal behaviour typical of RSL applications, normalized statistics for different scalars may not be equal, violating scalar similarity. Evaluating the degree to which statistics from measured time series approach this equality provides a test of scalar similarity. We will refer to the symptom of inequality of normalized statistics for different scalars as *dissimilarity*.

As with nonuniversal behaviour, scalar dissimilarity can result from surface heterogeneity (De Bruin et al. 1991; Roth and Oke 1995; Katul et al. 1995; Sempreviva and Højstrup 1998). Scalar dissimilarity, however, results from the more specific condition in which the heterogeneous distribution of one scalar source field is not the same as the heterogeneous distribution of another scalar source field. In accordance with this

theory, spatial separation of sources for heat and water vapour has been identified as a cause of dissimilarity between T and q transport, evidenced by a higher correlation coefficient ρ_{wT} as compared to ρ_{wq} for applications in the RSL over a patchy urban surface (Roth and Oke 1995), and over an uneven-aged forest, a uniform-irrigated bare soil, and a grass field (Katul et al. 1995). As with velocity-scalar correlations, analysis of the correlation of scalar fluctuations (e.g. $\rho_{Tq} = \pm 1$) has long been used in diagnosing turbulent exchange processes (e.g. Swinbank and Dyer 1967; Wesely 1976; Wyngaard et al. 1978), and is also useful in detecting the influence of heterogeneity in surface properties on scalar similarity (Wesely 1988; de Bruin et al. 1993; Roth and Oke 1995; Katul et al. 1995; Sempreviva and Højstrup 1998; Asanuma and Brutsaert 1999). This is demonstrated in Katul et al. (1995) in which decorrelation of T and q fluctuations observed over forest, bare soil, and grass covers is attributed to distinct source distributions for heat and water vapour, invalidating the flux-variance method for some conditions.

Sources of weakness in the application of similarity can be revealed by inspecting normalized energy spectra and scalar–scalar correlation for fluctuations associated with discrete eddy sizes, as similar scalars have, by definition, identical normalized energy spectra (Wesely 1988; Hill 1989). Such a scalewise analysis is useful as it identifies the length scales of heterogeneity that contribute to the divergence between measured and expected statistics. For example, cospectra of T and q from measurements over the marine surface layer indicated that boundary-layer scale eddies can inject joint scalar concentrations (e.g. T–q) from the temperature inversion (Phelps and Pond 1971) or downward transport of warm dry entrained air (Wyngaard et al. 1978) contributing to decorrelation or even sign reversal in surface measurements of the T–q correlation coefficients at large scales ($\approx$500 to 2000 m). Similarly, the T–q cospectrum measured in the RSL over an urban surface identified large-eddy convection as a source of decorrelation between T and q, as mixed layer air or air from above the capping inversion was exchanged with surface-layer sources (Roth and Oke 1995).

From this review we identify two ways in which the application of MOS in the RSL can fail, namely, nonuniversal behaviour and scalar dissimilarity. Clearly, universal scaling and scalar similarity are not expected when conditions of the MOS theory are violated. However, even when assumptions such as horizontal homogeneity are violated, the flux-variance approach may provide accurate flux estimates when scaled locally (i.e. site-specific MOS functions) to account for the effect of heterogeneity (Weaver 1990; Cellier and Brunet 1991; Bosveld 1997; Simpson et al. 1998; Mölder et al. 1999). Furthermore, some measurements conducted in the RSL suggest that scalar transport may be similar despite violations of the MOS assumption of horizontal homogeneity (Wesely 1988; Lloyd et al. 1991; Kustas et al. 1994; Simpson et al. 1998). Recognition of the potential for similarity theory to be partially upheld or corrected in some RSL applications leads us to introduce two classes of similarity: strong sense similarity (SSS) and weak sense similarity (WSS). SSS applies to cases in which the universal ASL similarity functions apply and scalar similarity is upheld with nearly equal normalized standard deviations. WSS applies to cases where similarity functions are nonuniversal, but scalar similarity is upheld and the empirical establishment of local corrections robustly relates fluxes to normalized statistics.

1.2 Senescence and the weakness of RSL similarity applications

In this study, we investigate how seasonal changes in forests may invalidate RSL similarity applications. This section discusses seasonal changes in forest structure and function that are likely to weaken the application of MOS in RSL applications.

Sources and sinks of carbon dioxide and water vapour are strongly coupled. Prior to senescence, the photosynthetically active canopy dominates daytime land-atmosphere water and carbon exchanges. Leaf surfaces provide a source of water and a sink of carbon dioxide (Fig. 1a) and the strength of both are regulated simultaneously by stomatal aperture (Ball et al. 1987; Wong et al. 1985a, b). Heat exchange occurs over all canopy surfaces (Campbell and Norman 1998) including surfaces that are relatively inactive in carbon and water exchange, such as woody tissue, although foliage intercepts most of the incoming radiation, making woody tissue a small contributor to forest-atmosphere heat exchange. Prior to leaf senescence in the mixed hardwood and conifer forest, sensible heat (H, $\mathrm{W\,m^{-2}}$), latent heat (LE, $\mathrm{W\,m^{-2}}$), and carbon dioxide (Fc, $\mu\mathrm{mol\,m^{-2}\,s^{-1}}$) are dominated by exchange between foliar surfaces and the atmosphere, nothing that LE is the product of evaporation (E) and the latent heat of vapourization (L). Hence turbulent events mix parcels that have scalar signatures originating from a similar distribution of T, q, and c sources and sinks prior to senescence. Spatial variation in leaf area density produces heterogeneity in the pre-senescence scalar source/sink fields at a length scale expected to be less than 10 m. This *branch scale* variability is reasonably well mixed by atmospheric turbulence, and has a relatively minor influence on the similarity application.

Senescence of deciduous foliage produces patchiness or heterogeneity associated with forest patches of photosynthetically active conifer stands and patches of respiring deciduous trees (Fig. 1b). LE and Fc are dominated by exchange over leaf, woody, and soil/litter surfaces with two distinct scalar signatures. In deciduous patches, soil and litter contribute small sources of water vapour and carbon dioxide $(+q, +c)$ from evaporation and respiration, while conifers provide a source of water vapour and sink of carbon dioxide $(+q, -c)$ from transpiration and photosynthesis. The length scale of this *patch scale* variability is expected to be larger than before senescence, on the order of a grove of trees, less than 100 m for the forests in this study. Deciduous and conifer canopies are both still sources of heat $(+T)$ despite senescence and abscission of deciduous foliage, with woody biomass and conifer foliage intercepting shortwave and longwave radiation. Senescence has the most pronounced effect on the carbon dioxide source/sink field as deciduous biomass shifts from a sink to a source. Taken together, senescence is expected to enhance departure from universal behaviour and lead to more pronounced dissimilarity between scalars. In addition, we expect to see the greatest influence of heterogeneity in the source/sink field for carbon dioxide, for which the contrast between deciduous and coniferous patches is strongest.

We hypothesize that a seasonal increase in canopy structural and functional heterogeneity introduces patchiness in scalar sources and sinks that causes the application of similarity theory in the RSL to shift from the WSS case to complete failure. To address this hypothesis we quantify the degree to which similarity theory is violated during and after deciduous senescence with two measures: departure between normalized standard deviations and those predicted from MOS, and divergence between normalized standard deviations of different scalars (Sect. 3.1). We also hypothesize that heterogeneity in scalar source/sink fields weakens the RSL application of similarity for specific ranges of length scales of turbulent mixing, owing to the introduction of

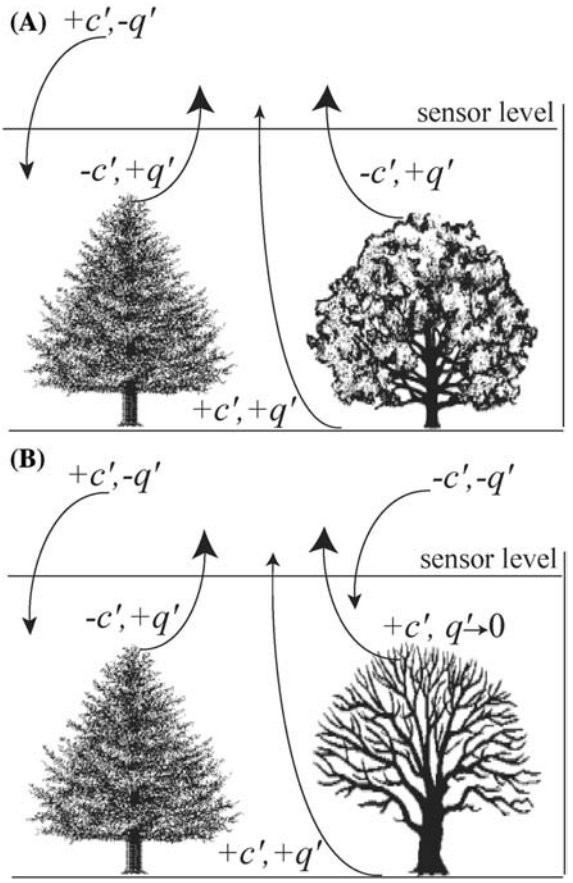

Fig. 1 Conceptual model of forest-atmosphere exchanges for a pre-senescent period (**A**) when both coniferous and deciduous vegetation contribute sources of water vapour and sinks of carbon dioxide relative to the atmosphere, and for a post-senescent period (**B**) when deciduous vegetation is a source of carbon dioxide relative to the atmosphere. The sign on primed scalars (c', q') indicates enrichment (+) or depletion (−) relative to a temporal average concentration at the sensor level (e.g. $+q'$ represents air enriched in water vapour). The below-canopy environment contributes sources of c and q

a local form of scalar–scalar correlation that interferes with a background, large-scale correlation of another form. This hypothesis is addressed with the scalewise evaluation of scalar–scalar correlations (Sect. 3.2), and investigated in greater detail with analysis of the scatter of scalar fluctuations associated with specific eddy sizes (Sect. 3.3). As such, we intend to identify specific length scales of mixing that appear to be most influenced by heterogeneity in scalar source fields.

2 Data collection

Field data were collected on a 37-m permanent walk-up tower in a mixed-hardwood forest of the Virginia Forest Research Facility (VFRF) and a 30-m tower in the Hardwood Division of the Duke Forest (HD). The VFRF is situated near Charlottesville, Virginia, U.S.A. approximately 80 km east of the Shenandoah Mountains and includes 80% hardwoods such as white, red, spanish, and black oaks (30%), red maple (21%), mockernut and pignut hickory (6%), and tulip poplar (6%), and 20% conifers including Virginia and longleaf pines and some juniper with a maximum tree age approximately 60 years old and an average canopy height of 22 m.

Measurements at the VFRF were conducted from day of year (DOY) 279–286 of 2000 before deciduous tree leaf senescence and abscission, and from DOY 310–320 of 2000 after leaf abscission. The HD forest is an uneven-aged stand approximately 80–100 years old, approximately 25 m tall with about 300 trees per hectare, a basal area of 26 m^2 ha^{-1}, and composed primarily of oak and hickory with sparse (< 15%) loblolly pine, and a few tulip poplar and sweetgum trees. The HD data were obtained from DOY 140–365 of 2001. Streamwise horizontal velocity (u), transverse horizontal velocity (v), vertical velocity (w), T, c, and q were measured with a triaxial sonic anemometer (CSAT3, Campbell Scientific) and an open-path CO_2/H_2O infrared gas analyzer (IRGA) (7500, LI-COR) mounted 33 m and 36 m above the forest floor at VFRF and HD, respectively. High frequency data (10 Hz) were collected and data quality control and post-processing involved removal of data spikes, rotation of the flux tensor into the mean horizontal wind direction and to the plane where $\langle w \rangle = 0$, and a correction of water vapour and carbon dioxide fluxes based on Webb et al. (1980). Half-hour averaged fluxes of momentum, H, LE, and Fc were calculated as well as basic turbulence and micrometeorological statistics. The standard micrometeorological sign convention of positive fluxes from the surface to the atmosphere was adopted. Data analysis was performed on 30-min files that met specific selection criteria as outlined in Table 1. We restricted our analysis to near-neutral and unstable conditions. The minimum flux thresholds were selected because the normalized standard deviations become poorly defined as scalar flux vanishes. The friction velocity, u_*, and turbulence intensity ($\frac{\sigma_u}{\langle u \rangle}$, where σ_u is the temporal standard deviation of u, and $\langle \cdot \rangle$ is the time-average operator) thresholds omit files from analysis if the turbulence is poorly developed or when Taylor's (1938) frozen turbulence hypothesis is certain to be violated. The atmospheric stability parameter, ζ, was estimated with d_o of 0.7 h (Campbell and Norman 1998), and an Obukhov (1946) length, L_o, calculated as

$$L_o = -\nu u_*^3 / [kg(H/TC_p + 0.61E)],$$

where ν is the density of air, g is the acceleration due to gravity, C_p is the specific heat capacity of air, L is the latent heat of vapourization, and k is von Karman's constant taken to be 0.41 (Monin and Yaglom 1971).

Table 1 Conditions for selection of 30-min files, and the number of files selected for the VFRF and HD sites both pre- and post-senescence (N pre / N post)

Measure	Condition
$\sigma_u/\langle u \rangle$	< 0.8
ζ	$-100 < \zeta < 0$
u_* (m s^{-1})	> 0.1
LE (W m^{-2})	$\lvert LE \rvert > 10$
H (W m^{-2})	$\lvert H \rvert > 10$
Fc (μmol m^{-2} s^{-1})	$\lvert Fc \rvert > 2$
VFRF: N pre / N post	65 of 253 / 16 of 198
HD: N pre / N post	916 of 3552 / 272 of 2352

3 Results and discussion

3.1 Examining weakness in similarity with senescence

To evaluate the first hypothesis, we first assess the fit of normalized standard deviations from our RSL observations to the proposed universal MOS functions over a wide range of unstable conditions. Figure 2 shows normalized standard deviations (e.g. σ_T/T_*, where $T_* = \langle w'T'\rangle/u_*$, where the prime denotes a fluctuation from the mean) for T, q, and c plotted as a function of stability for near-neutral to unstable conditions both before and after senescence from the VFRF experiment. Normalized standard deviations for T, q, and c are elevated above proposed universal similarity functions for scalars, for example, $(2(1+9.5|\zeta|)^{-1/3})$ taken from Kaimal and Finnigan (1994) and plotted as the dashed line in Fig. 2. The post-senescence normalized standard deviations are generally higher than those for the pre-senescence period for a given stability, likely owing to added heterogeneity in the surface cover, which has been identified as a likely cause of elevated normalized standard deviations for RSL applications by Weaver (1990) and Katul et al. (1995).

Away from the neutral limit towards unstable conditions, scalar transport phenomenology predicts a power law decrease of normalized standard deviations for scalars as a function of increasing instability according to $\zeta^{-1/3}$ (e.g. Albertson et al. 1995). This decay with ζ is upheld for pre-senescence observations despite elevated normalized standard deviations (Fig. 2), indicating that mild heterogeneity associated with the pre-senescence forest source sink distribution did not structurally alter the effect of stability on flux-variance similarity. Unfortunately, lack of data prohibits assessment of the influence of senescence on power law scaling at the VFRF site.

In summary, the results from the VFRF experiment (Fig. 2) suggest that the RSL application of similarity theory was weakened through senescence for all three scalars.

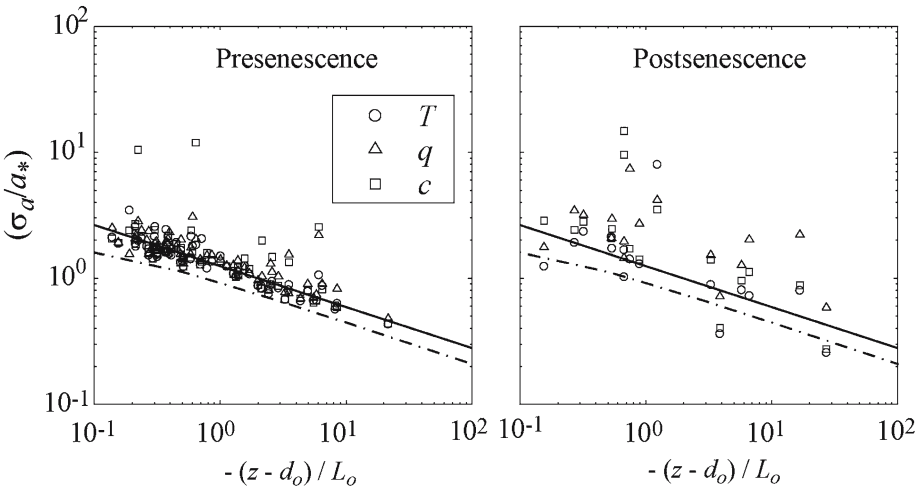

Fig. 2 Normalized standard deviations for T, q, and c for near-neutral to unstable conditions both before and after senescence measured at VFRF. The dashed line indicates the flux-variance similarity function for T reported in Kaimal and Finnigan (1994), and the solid line presents the regression of σ_T/T_* versus $-\zeta$ from the pre-senescence observations (reproduced as a reference in the post-senescence panel)

However, the spread of the data and the small number of observations preclude generalization from the observations obtained at this site alone. Hence, we introduce a more extensive dataset from the Hardwood Division of the Duke Forest, also allowing us to investigate the generality of findings from the VFRF. Two periods are selected to represent a contrast between low and high spatial variability of scalar sources/sinks, assessed with litterfall-based leaf area index (LAI; m^2 leaf m^{-2} ground) as estimated by the Duke Hardwood Division research group. The first period (DOY 150–225) includes observations conducted during peak leaf area index (LAI) when the spatial variability in forest structure and function is relatively low, and the second period (DOY 275–325) includes observations during senescence at the end of the growing season as leaf area declines, causing increased spatial variability in scalar source/sink distributions.

As found with the VFRF data, normalized standard deviations are elevated well above the universal ASL predictions during both the peak LAI and declining LAI periods at the HD site, shown here with averages over bins of stability owing to the much larger number of samples (Table 1), which would cloud interpretation if displayed individually (Fig. 3). Also in agreement with the VFRF data, the HD data show that power law scaling of normalized standard deviations as a function of ζ is robust to changes in LAI from the peak and declining LAI periods for T and q while c deviates from the anticipated form (Fig. 3). General nonuniversal behaviour of normalized standard deviations in the RSL for the two sites indicates failure of SSS both before and after senescence, with more pronounced departure from universal behaviour during the seasonal decline in deciduous productivity.

Having documented the failure of SSS due to the elevation of normalized standard deviations, we now investigate the influence of senescence on scalar similarity to determine whether WSS is upheld. Again inspecting Fig. 3, throughout senescence and the decline in LAI, normalized standard deviations for T and q are similar to those during peak LAI, although the average σ_c/c_* is markedly elevated for the full range of stability, suggesting that heterogeneity in c sources/sinks increases with senescence more than that for both T and q.

Figure 4 summarizes the effect of heterogeneity on the validity of the universal and scalar similarity assumptions for the HD data by showing 10-day moving averages of (a) the departure of scalar normalized standard deviations from their expected value based on stability, represented by E, (b) ratios of scalar normalized standard deviations, as well as temporal trends of (c) LAI, and (d) mean daytime Fc. The magnitude of mean daytime Fc decreases from approximately DOY 230–310 as deciduous photosynthesis diminishes, with a succeeding decline in LAI (Fig. 4). Associated with this decline in LAI, normalized standard deviations for q and c increase, with the most pronounced increase for c (Figs. 3, 4), likely due to stronger contrasts between deciduous and coniferous patches for the c source/sink field as compared to the q field. In contrast, the normalized standard deviation of T decreases through the decline in LAI, likely associated with a more active role of T in turbulence dynamics due to the seasonal decrease in average air temperature. Heterogeneity associated with senescence also appeared to contribute to dissimilarity between scalars, as evidenced by the marked increase of the ratio of normalized standard deviations, expected to be unity for similar scalars (Fig. 4).

From this analysis we conclude that our first hypothesis is correct. Prior to senescence, WSS was upheld, as factors causing nonuniversal behaviour did not result in scalar dissimilarity. In contrast, seasonal changes in forest structure and function

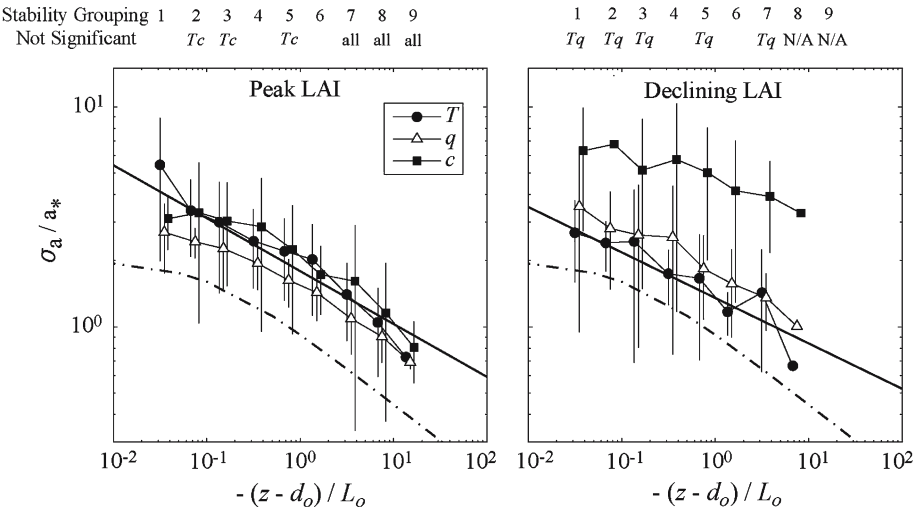

Fig. 3 Normalized standard deviations for T, q, and c for near-neutral to unstable conditions for the peak and declining LAI periods at HD. Symbols and vertical lines represent the mean and standard deviations for measured normalized standard deviations within ranges of stability $(-(z - d_o)/L_o)$, and symbols for T and c are slightly offset in the x-direction for clarity. The dashed lines indicates the flux-variance similarity function for T reported in Kaimal and Finnigan (1994), and the solid lines present regressions of σ_T/T_* vs. $-\zeta$. Shown above are results of two-tailed, heteroscedastic Student's t-tests contrasting normalized standard deviations between the three scalars for each stability grouping, where 'Not Significant' refers to contrasts for which P-values exceed 0.05 and Tc, Tq, and 'all' represent lack of significant differences for contrasts between normalized standard deviations for T and c, T and q, or all three contrasts, respectively, while N/A represents not applicable due to lack of data

during the senescence of deciduous vegetation initiated a transition from the WSS condition to complete failure of the RSL similarity application. Hence, increased patchiness in forest structure and function associated with the seasonal cycle appears to be an important factor in the validity of scalar similarity in RSL applications, particularly with regard to CO_2.

In addition to variability between source fields of heat, moisture, and carbon dioxide, $T-q$ and $T-c$ dissimilarities may also arise from their contrasting roles as active (T) versus passive (q, c) scalars. Fluctuations of q, as a passive scalar, have been shown to be influenced by source distributions of both heat and moisture, whereas fluctuations of T are only under the influence of the heat source distribution (Katul et al. 1995; Asanuma and Brutsaert 1999; Katul and Hsieh 1999). Furthermore, T, being an active scalar, influences the turbulence field through buoyancy production of turbulent kinetic energy, unlike the passive scalars of moisture and carbon dioxide (Asanuma and Brutsaert 1999; Katul and Hsieh 1999). With this in mind, it is not surprising to see that normalized standard deviations for T are relatively low compared to those for q and c, though we note that T and q normalized standard deviations were not significantly different during the declining LAI period (Fig. 4). In addition, the seasonal decrease in surface fluxes, particularly for carbon dioxide, offers an additional possible explanation for observed dissimilarity between scalars. Thus, while the temporal transition from similar to dissimilar behaviour is strongly associated with senescence, these additional transients provide alternative explanations. To further

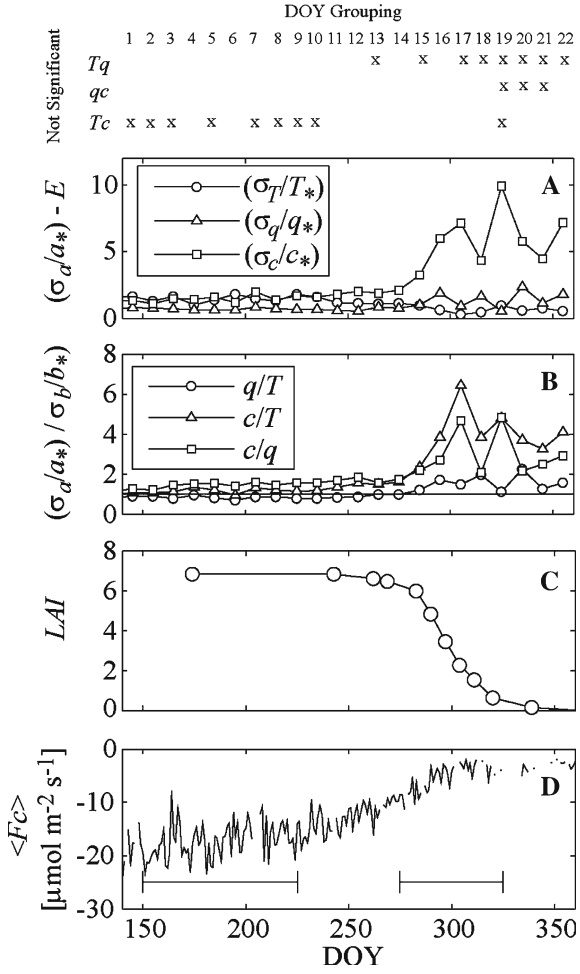

Fig. 4 Ten-day moving average of (**A**) normalized standard deviations for T, q, and c, minus their expected value based on stability (E), (**B**) the ratio of normalized standard deviations for q with T, c with T, and c with q, as well as temporal trends of (**C**) leaf area index (LAI) and (**D**) mean daytime carbon dioxide flux (Fc) all presented for day of year (DOY) 140–365 in 2001 at HD. At top are results of two-tailed Student's t-tests contrasting stability adjusted normalized standard deviations (as in **A**) between the three scalars for each DOY grouping, where 'x' indicates contrasts for which P-values exceed 0.05 for Tq, Tc, or qc, representing contrasts between T and q, T and c, and q and c, respectively

diagnose the cause of dissimilarity we now introduce a scalewise analysis of scalar fluctuations and their correlations.

3.2 Investigating scalewise departure from scalar similarity

To better understand the source of weakness in the similarity application in the RSL, we inspect the influence of forest patchiness at VFRF on correlations between scalars as a function of eddy diameter. In the ASL over a homogeneous surface, the scalewise correlation between scalars is expected to remain at unity for all scales. However, in the RSL over a heterogeneous surface, the scalar source/sink field may exhibit spatial variability at scales smaller than those of turbulence production, thus perturbing the scalar–scalar correlation within the inertial range. This can be considered as a contamination of the correlation passed from large scales.

To evaluate our second hypothesis, which states that heterogeneity in scalar source/sink fields influences the RSL similarity application for specific length scales of mixing, we use an orthonormal wavelet decomposition into scale and position. The orthogonal, discrete wavelet transform can be applied to a time series $f(t)$ to obtain

the wavelet coefficients $WC\,(j,m)$ centred at nonoverlapping positions j in the time series where $j = (2^m i + 1)/2$, and for each scale m where $m = 1, 2, \ldots, M$, and 2^M is the total number of measurements in the time series (Katul and Parlange 1995; Scanlon and Albertson 2001). We use the Haar wavelet basis because it is well suited for identifying features of turbulent energy and scalar time series (Katul and Vidakovic 1996, 1998). Using Taylor's (1938) "frozen turbulence" hypothesis, each scale index m is converted into eddy diameters, r_m [m], with:

$$r_m = \frac{2^m \langle u \rangle}{f_s}, \tag{1}$$

where f_s is the measurement frequency (s^{-1}). We note that the frozen turbulence hypothesis is best applied when turbulence intensity ($\frac{\sigma_u}{\langle u \rangle}$) is low as steady convection velocities provide a better preservation of upstream turbulence structure (Lumley 1965). With the wavelet transformation of scalar time series, we calculate the correlation between scalars associated with specific eddy diameters, as

$$\rho_{ab}\,(r_m) = \frac{\left[\sum_{j=1}^{2^{M-m}} [WC'_a(j,m)][WC'_b(j,m)]\right] \frac{1}{2^{M-m}}}{\sigma_a(m)\sigma_b(m)}, \tag{2}$$

where subscripts a and b refer to hypothetical scalars, $WC'_a(j,m)$ is the deviation of a wavelet coefficient at scale j from the mean WC_a(m), and $\sigma_a(m)$ and $\sigma_b(m)$ are the standard deviations of the wavelet coefficients at scale m (Scanlon and Albertson 2001).

Prior to senescence, scalewise correlation between scalars is conservative through much of the production range, as T–q, T–c, and c–q correlations are close to unity (± 1) for eddies of sizes ~ 10 to 1000 m (Fig. 5). At the largest resolved eddy sizes ($r_m \sim 10^3$ m), correlations between scalars are lower than at the intermediate scales (1–100 m), likely resulting from nonstationarity or large-scale processes, such as entrainment fluxes (e.g. De Bruin et al. 1993, 1999; Sempreviva and Gryning 2000). At the smallest resolved scales ($r_m < 1$ m), instrument separation of the sonic anemometer and infrared gas analyzer can partially account for lower T–q and T–c correlations as compared to q–c correlation. Still, loss of correlation between scalars is evident for eddies of order 10^1 m in diameter and continues toward smaller scales, suggesting that even for the pre-senescence forest, the influence of small-scale heterogeneity was strong at the scales of variation in vegetation density, previously identified as *branch scales* (Sect. 1.2).

Scalewise correlations between scalars for the post-senescence period are weaker than those for pre-senescence for all resolved eddy sizes. A particularly large difference is evident for eddies ranging from 0.5 to 10 m (Fig. 5), with a reduction even for production range scales (~ 10 to 1000 m) for which scalar similarity is expected to be most reliable in the near-surface turbulence (ASL and RSL), as found for the pre-senescence period. Thus, the temporal increase in patchiness associated with senescence decorrelates scalar fluctuations, with a peak difference at the *branch* scales of order 10^0 m, but also evident at *patch* scales of around 10^2 m. While, we cannot conclude that local surface heterogeneity contaminates the scalar–scalar correlation in the inertial subrange, as posed in our second hypothesis, these findings speak more generally to the pronounced effects of a seasonal increase in heterogeneity that decorrelates scalar fluctuations thus weakening RSL similarity applications.

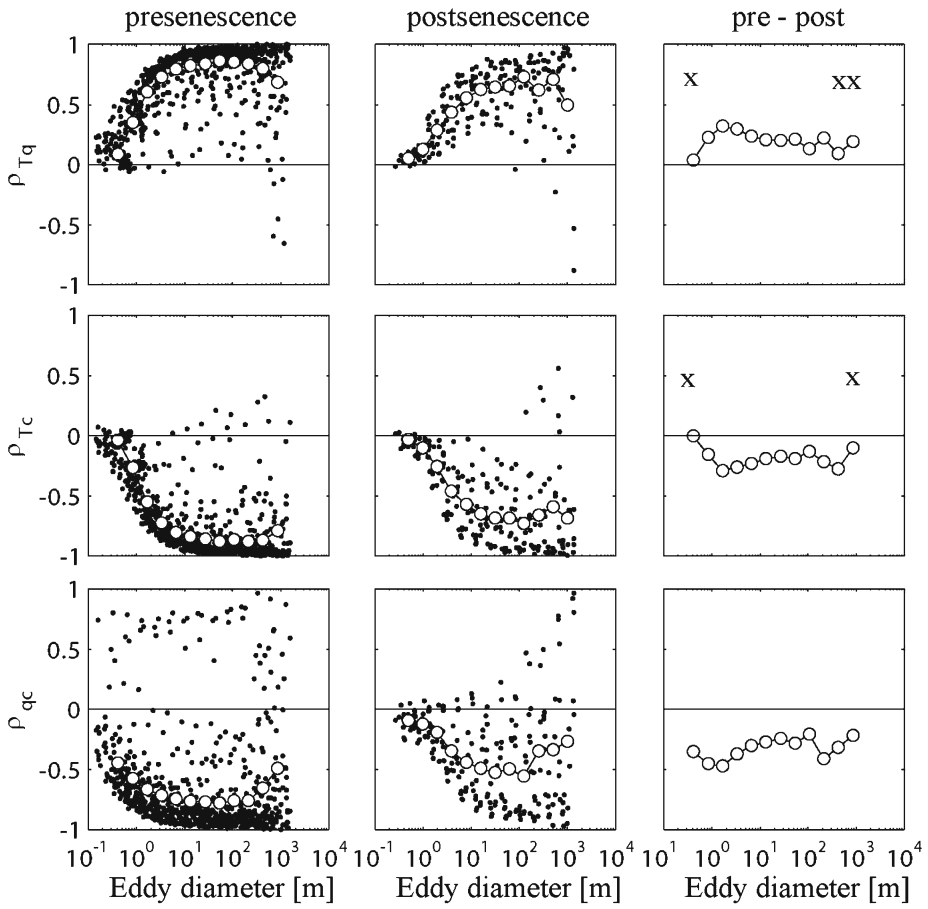

Fig. 5 Cross-correlations for T–q, T–c, and q–c over the eddy diameter showing half-hourly (*closed symbols*) data, and bin-averages over eddy diameter (open symbols) both pre-senescence and post-senescence, as well as pre-senescence minus post-senescence (pre–post) bin-averaged scalar–scalar spectral correlations all for VFRF. Results of two-tailed, heteroscedastic Student's t-tests contrasting pre- and post-senescence cross-correlations are shown with 'x' above mean differences (*right panels*) indicating P-values that exceeded 0.05

Up to this point, we have reported statistics commonly used to investigate whether MOS is upheld. While revealing, this approach allows us only to infer the cause of nonuniversal or dissimilar behaviour. A more in-depth analysis of high frequency scalar time series may provide a stronger case for attributing the failure of this RSL similarity application to surface heterogeneity, as examined in the final section.

3.3 Diagnosing effects of heterogeneity on scalar similarity

To more closely examine the effects of surface heterogeneity on the similarity application we inspect scatter plots of scalar fluctuations for discrete eddy scales for two representative half-hour files from the VFRF dataset, one pre-senescence and one post-senescence, with similar atmospheric conditions and vertical fluxes (Table 2). We obtain scalar fluctuations for discrete scales by applying a wavelet band-pass filter.

Table 2 Atmospheric conditions and fluxes for two half-hour files selected as case studies for the pre- and post-senescent periods

Measure	Pre	Post
time of day	1500	1500
$\sigma_u/\langle u\rangle$	0.43	0.52
ζ	−0.45	−0.22
u_* (m s^{-1})	0.31	0.41
H (W m^{-2})	55	63
LE (W m^{-2})	104	172
Fc (μmol m^{-2} s^{-1})	−6.4	3.2

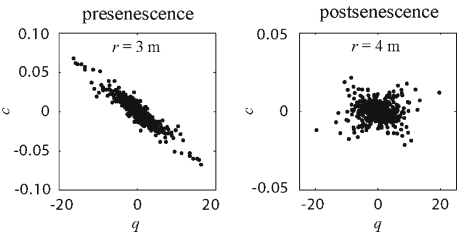

Fig. 6 Scatter of scalar fluctuations for c and q for discrete eddy diameters (r) from a pre-senescence and a post-senescence period obtained with a band-pass filter of wavelet coefficients for two half-hour files from VFRF

Figure 6 shows the scatter of c and q fluctuations for eddy diameters of approximately 4 m, the scale of the peak difference between pre- and post-senescence scalewise correlations between scalars (Fig. 5). Unlike pre-senescence, the post-senescence scatter of c and q indicates a mixture of signatures of contrasting signs (Fig. 6). This finding is consistent with the daytime contrast between coniferous and defoliated deciduous patches imprinting the correlation of carbon dioxide and water vapour fluctuations with negative and positive signs, respectively (Fig. 1). Hence, a mixture of scalar–scalar signatures arising from increased surface contrast in the senescent deciduous–coniferous forest leads to failure of similarity for this RSL application.

4 Conclusions

Elevation of normalized standard deviations obtained from RSL measurements relative to forms proposed to be universal for ASL applications indicated the failure of *strong sense similarity* for the RSL application both before and after deciduous senescence over the two mixed hardwood deciduous and conifer forests. Observations before senescence could be characterized as having met the conditions for *weak sense similarity*, as general adherence to power law scaling of normalized standard deviations with stability, and good agreement between normalized standard deviations of different scalars indicated that a site-specific (i.e. weak) scalar similarity was upheld despite nonuniversal behaviour. Seasonal changes in canopy structure and function at the same site shifted scalar transport from a condition of weak sense similarity to complete failure of the similarity application in the RSL. This failure is attributed to the divergence of source/sink distributions for different scalars, causing scalar transport to be dissimilar, with particularly marked dissimilarity between carbon dioxide and the other two scalars, namely temperature and water vapour. Prior to senescence, correlation of scalar fluctuations as a function of eddy sizes was near unity, with loss of correlation appearing for eddies smaller than about 10 m. Through senescence, scalar fluctuations were decorrelated and we noted a mixture of source/sink signatures in the

scalewise scatter of scalars. This suggests that a seasonal production of heterogeneity in scalar sources at the scale of hardwood or coniferous patches down to the scale of branches ($\sim$ 100 to 0.5 m) resulted in the production of scalar covariance over a broad range of eddy sizes. These temporal changes in forest structure and function through senescence weaken the application of scalar similarity in the RSL. During such periods, when the assumptions of MOS are strongly violated, a more complicated scalar transport phenomenology is required to capture the influence of spatial and temporal heterogeneity occurring over a wide range of scales, issuing caution for the use of techniques that rely on similarity assumptions in the roughness sublayer.

Acknowledgements This research was supported by the Office of Science Biological and Environmental Research (BER) Program, U.S. Department of Energy, through the Southeast Regional Center (SERC) of the National Institute for Global Environmental Change (NIGEC) under Cooperative Agreement No. DE-FC03-90ER61010. In addition, we thank Gabriel Katul, Ram Oren, Paul Stoy, and Karina Shäfer all at Duke University for making the Hardwood Division data available, made possible also through support from the Office of Science (BER) Program, U.S. Department of Energy, through SERC of NIGEC under Cooperative Agreement No. DE-FC02-03ER63613, and through the Terrestrial Carbon Processes Program (TCP). The authors thank Jose Fuentes at the University of Virginia for logistical support at the Virginia Forest Research Facility.

References

Albertson JD, Parlange MB, Katul GG, Chu C-R, Stricker H, Tyler S (1995) Sensible heat flux from arid regions: a simple flux-variance method. Water Resour Res 31(4):969–973

Andreas EL, Hill RJ, Gosz JR, Moore DI, Otto WD, Sarma AD (1998) Statistics of surface-layer turbulence over terrain with metre-scale heterogeneity. Boundary-Layer Meteorol 86:379–408

Asanuma J, Brutsaert W (1999) Turbulence variance characteristics of temperature and humidity in the unstable atmospheric surface layer above a variable pine forest. Water Resour Res 35(2):515–521

Ball JT, Woodrow IE, Berry JA (1987) A model predicting stomatal conductance and its contribution to the control of photosynthesis under different environmental conditions. In: Biggens J (ed) Progress in photosynthesis research, Martinus Nijhoff Publishers, Dordrecht, Netherlands Vol IV. pp 221–224

Bosveld FC (1997) Derivation of fluxes from profiles over a moderately homogeneous forest. Boundary-Layer Meteorol 84:289–327

Brutsaert W (1982) Evaporation into the atmosphere. D. Riedel Publishing Company, Dordrecht, Holland, 299 pp

Businger JA, Wyngaard JC, Izumi Y, Bradley EF (1971) Flux-profile relationships in the atmospheric surface layer. J Atmos Sci 28:181–189

Campbell GS, Norman JM (1998) An introduction to environmental biophysics, 2nd edn. Springer, New York, 286 pp

Cellier P, Brunet Y (1992) Flux-gradient relationships above tall plant canopies. Agric For Meteorol 58:93–117

Denmead OT, Bradley EF (1985) Flux-gradient relationships in a forest canopy. In: Hutchison BA, Hicks BB (eds) The forest-atmosphere interaction. D. Reidel Publishing Co., Dordrecht, pp 421–442

De Bruin HAR, Bink NJ, Kroon LJ (1991) Fluxes in the surface layer under advective conditions. In: Schmugge TJ, André JC (eds) Workshop on land surface evaporation, measurement and parameterization. Springer, New York, pp 157–169

De Bruin HAR, Kohsiek W, Van Den Hurk BJJM (1993) A verification of some methods to determine the fluxes of momentum, sensible heat and water vapour using standard deviation and structure parameter of scalar meteorological quantities. Boundary-Layer Meteorol 63:231–257

De Bruin HAR, Van Den Hurk BJJM, Kroon LJJM (1999) On the temperature-humidity correlation and similarity. Boundary-Layer Meteorol 93:453–468

Dias NL, Brutsaert W (1996) Similarity of scalars under stable conditions. Boundary-Layer Meteorol 80:355–373

Dyer AJ (1974) A review of flux-gradient relationships. Boundary-Layer Meteorol 7:363–372
Garratt JR (1978) Flux profile relations above tall vegetation. Quart J Roy Meteorol Soc 104:199–211
Garratt (1980) Surface influence upon Vertical Profiles in the atmosphere near-surface layer. Quart J Roy Meteorol Soc 106:803–819
Hsieh C-I, Katul GG, Schieldge J, Sigmon J, Knoerr KR (1996) Estimation of momentum and heat fluxes using dissipation and flux-variance methods in the unstable surface layer. Water Resour Res 32(8):2453–2462
Hill RJ (1989) Implications of Monin and Obukhov similarity theory for scalar quantities. J Atmos Sci 46:2236–2244
Högström U, Bergström H, Smedman A-S, Halldin S, Lindroth A (1989) Turbulent exchange above a pine forest, I: fluxes and gradients. Boundary-Layer Meteorol 49:197–217
Kaimal JC, Finnigan JJ (1994) Atmospheric boundary layer flows. Oxford University Press, New York, 289 pp
Katul GG, Parlange MB (1995) Analysis of land surface heat fluxes using the orthonormal wavelet approach. Water Resour Res 31:2743–2749
Katul GG, Vidakovic B (1996) The partitioning of the attached and detached eddy motion in the atmospheric surface layer using Lorentz wavelet filtering. Boundary-Layer Meteorol 77:153–172
Katul GG, Vidakovic B (1998) Identification of low-dimensional energy containing/flux transporting eddy motion in the atmospheric surface layer using wavelet thresholding methods. J Atmos Sci 54:91–103
Katul GG, Goltz SM, Hsieh C-I, Cheng Y, Mowry F, Sigmon J (1995) Estimation of surface heat and momentum fluxes using the flux-variance method above uniform and non-uniform terrain. Boundary-Layer Meteorol 74:237–260
Katul GG, Hsieh C-I, Oren R, Ellsworth D, Phillips N (1996) Latent and sensible heat flux predictions from a uniform pine forest using surface renewal and flux variance methods. Boundary-Layer Meteorol 80:249–282
Katul GG, Hsieh C-I (1999) A note on the flux-variance similarity relationships for heat and water vapour in the unstable atmospheric surface layer. Boundary-Layer Meteorol 90:327–338
Kustas WP, Blanford JH, Stannard DI, Daughtry CST, Nichols WD, Weltz MA (1994) Local energy fux estimates from unstable conditions using variance data in semiarid rangelands. Water Resour Res 30:1351–1361
Lloyd CR, Culf AD, Dolman AJ, Gash JH (1991) Estimates of sensible heat flux from observations of temperature fluctuations. Boundary-Layer Meteorol 57:311–322
Lumley JL (1965) Interpretation of time spectra measured in high-intensity shear flows. Phy Fluids 8:1056–1062
Mahrt L (2000) Surface heterogeneity and the vertical structure of the boundary layer. Boundary-Layer Meteorol 96:33–62
McNaughton KG, Laubach J (1998) Unsteadiness as a cause of non-equality of eddy diffusivities for heat and vapour at the base of an advective inversion. Boundary-Layer Meteorol 88:479–504
Mölder M, Grelle G, Lindroth A, Halldin S (1999) Flux-profile relationships over a boreal forest – roughness sublayer corrections. Agric For Meteorol 98–99:645–658
Monin AS, Obukhov AM (1954) Basic laws of turbulent mixing in the atmospheric surface layer. Trans Geophys Inst Akad Nauk USSR 24(151):163–187
Monin AS, Yaglom AM (1971) Statistical fluid mechanics: mechanics of turbulence, Vol 1. J. L. Lumley (ed). MIT Press, Cambridge, 769 pp
Obukhov AM (1946) Turbulentnost v temperaturnoj - neodnorodnoj atmosfere (Turbulence in an atmosphere with a non-uniform temperature). Trudy Inst Theor Geofiz An SSSR 1 1:95–115
Obukhov AM (1960) O structure temperaturnogo polja i polja skorostej v uslovijach konveckcii (Structure of the temperature and velocity fields under conditions of free convection). Izv AN SSSR, ser Geofiz 9:1392–1396
Padro J (1993) An investigation of flux-variance methods and universal functions applied to three land-use types in unstable conditions. Boundary-Layer Meteorol 66:413–425
Phelps GT, Pond S (1971) Spectra of the temperature and humidity fluctuations and of the fluxes of moisture and sensible heat in the marine boundary layer. J Atmos Sci 28:918–928
Raupach MR (1979) Anomalies in flux-gradient relationships over forest. Boundary-Layer Meteorol 16:467–486
Raupach MR, Finnigan JJ, Brunet Y (1996) Coherent eddies and turbulence in vegetation canopies: the mixing-layer analogy. Boundary-Layer Meteorol 78(3–4):351–382
Rotach MW (1999) Turbulence close to a rough urban surface Part II: variances and gradients. Boundary-Layer Meteorol 66:75–92

Roth M, Oke TR (1995) Relative efficiencies of turbulent transfer of heat, mass, and momentum over a patchy urban surface. J Atmos Sci 52(11):1863–1874
Scanlon TM, Albertson JD (2001) Turbulent transport of carbon dioxide and water vapour within a vegetation canopy during unstable conditions: identification of episodes using wavelet analysis. J Geophys Res 106(D7):7251–7262
Sempreviva AM, Højstrup J (1998) Transport of temperature and humidity variance and covariance in the marine surface layer. Boundary-Layer Meteorol 87:233–253
Sempreviva A, Gryning S-E (2000) Mixing height over water and its role on the correlation between temperature and humidity fluctutations in the unstable surface layer. Boundary-Layer Meteorol 97:273–291
Simpson IJ, Thurtell GW, Neumann HH, den Hartog G, Edwards GC (1998) The validity of similarity theory in the roughness sublayer above forests. Boundary-Layer Meteorol 87:69–99
Swinbank WC, Dyer AJ (1967) An experimental study in micrometeorology. Quart J Roy Meteorol Soc 93:484–500
Taylor GI (1938) The spectrum of turbulence. Proc R Soc London A 164:476–490
Thom AS, Stewart JB, Oliver HR, Gash JHC (1975) Comparison of aerodynamic and energy budget estimates of fluxes over a pine forest. Quart J Roy Meteorol Soc 101:93–105
Tillman JE (1972) The indirect determination of stability, heat and momentum fluxes in the atmospheric boundary layer from simple scalar variables during dry unstable conditions. J Appl Meteorol 11:783–792
Warhaft Z (2000) Passive scalars in turbulent flows. Annu Rev Fluid Mech 32:203–240
Weaver HL (1990) Temperature and humidity flux-variance relations determined by one-dimensional eddy correlation. Boundary-Layer Meteorol 53:77–91
Webb EK, Pearman GI, Leuning R (1980) Correction of flux measurements for density effects due to heat and water vapour transfer. Quart J Roy Meteorol Soc 106:85–100
Wesely ML (1976) Combined effect of temperature and humidity fluctuations on refractive index. J Appl Meteorol 15:43–49
Wesely ML (1988) Use of variance techniques to measure dry air-surface exchange rates. Boundary-Layer Meteorol 44:13–31
Wong S-C, Cowan I, Farquhar GD (1985a) Leaf conductance in relation to rate of CO_2 assimilation: I. Influence of nitrogen nutrition, phosphorus nutrition, photon flux density, and ambient partial pressure of CO_2 during ontogeny. Plant Phys 78:821–825
Wong S-C, Cowan I, Farquhar GD (1985b) Leaf conductance in relation to rate of CO_2 assimilation: III. Influences of water stress and photoinhibition. Plant Phys 78:830–834
Wyngaard JC, Pennell WT, Lenschow DH, LeMone MA (1978) The temperature-humidity covariance budget in the convective boundary layer. J Atmos Sci 35:47–58